[redacted] #1

Report 1669

DEPARTMENT OF THE NAVY

DAVID TAYLOR MODEL BASIN

[redacted]

HYDROMECHANICS

o

AERODYNAMICS

o

STRUCTURAL MECHANICS

o

APPLIED MATHEMATICS

BODIES OF REVOLUTION WITH HIGH CAVITATION-INCEPTION SPEEDS - FOR APPLICATION TO THE DESIGN OF HYDROFOIL-BOAT NACELLES

by

Wilburn L. Moore

[redacted]

HYDROMECHANICS LABORATORY
RESEARCH AND DEVELOPMENT REPORT

September 1962

Report 1669

BODIES OF REVOLUTION WITH HIGH CAVITATION-INCEPTION SPEEDS - FOR APPLICATION TO THE DESIGN OF HYDROFOIL-BOAT NACELLES

by

Wilburn L. Moore

September 1962

Report 1669
S-F013-0201

TABLE OF CONTENTS

LIST OF FIGURES

LIST OF TABLES

NOTATION

C_p	Prismatic coefficient of bodies = $\frac{\text{Volume}}{1/4\pi D^2 L}$
D	Maximum diameter of body
L	Length of body
m	Dimensionless location of maximum section along axis
p	Local pressure on the body
p_A	Atmospheric pressure
p_H	Free-stream pressure due to submergence
p_V	Vapor pressure of water
V	Free-stream velocity
v	Local velocity
X	Distance to section from nose
Y	Radial offset of nacelle measured from axis of symmetry
ρ	Density of water
σ_i	Incipient-cavitation number

ABSTRACT

The potential velocity distributions of some promising bodies of revolution from the aeronautical and hydrodynamic literature are compared as part of a project to present design data for hydrofoil-boat nacelles. From the potential velocity distributions, cavitation-inception speeds, based on pressure only, are predicted for each shape. A DTMB Series 58 form, Model 4162, is judged most promising for hydrofoil-boat application.

INTRODUCTION

The David Taylor Model Basin proposed making a systematic study to determine combinations of hydrofoil craft components with high cavitation-inception speeds and low drag. This study was to include both theoretical and experimental work and was authorized by the Bureau of Ships[1] as part of the Hydrofoil Accelerated Program.

A previous DTMB report[2] discussed the pressure distributions and drag characteristics of the bodies of revolution of DTMB Series 58 to determine their application to the design of hydrofoil-boat nacelles.

In this report, two promising Series 58 shapes are compared with three promising shapes from the hydrodynamic and aeronautical literature. These comparisons are based on potential theory pressure distributions which are used to predict cavitation-inception speeds. The method used to calculate the pressure distributions is due to Smith and Pierce.[3] Results from this method are compared with experimental results and other theoretical results to show its application to this investigation.

Reference 2 indicated that nacelle drag is a small part of the total drag of a typical hydrofoil boat in the high-speed flying condition. Therefore, a compromise will not be sought in this report between an optimum drag shape and an optimum pressure-distribution shape. The shape that has

---

[1] References are listed on page 8.

the highest cavitation inception speed consistent with reasonably low drag will be considered most promising.

DESCRIPTION OF BODIES OF REVOLUTION

The following bodies of revolution with length-diameter ratios of 5, 6, and 7 are discussed:

1. A shape derived by Munzner and Reichardt to obtain a predominantly constant pressure distribution[4] (designated M-R).

2. The TMB-EPH form[5] (designated EPH).

3. A body of revolution generated by using offsets of the NACA 16-series airfoil section[6] (designated 16).

4. Two promising basic shapes of DTMB Series 58[7] (designated by their model numbers, 4165 and 4162).

References 8 and 9 discussed some shapes with promising pressure distributions as calculated by methods outlined therein. However, calculations by the Smith-Pierce method did not confirm the high cavitation-inception speeds predicted for these shapes by References 8 and 9.

References 10, 11, and 12 were also examined but the pressure distributions of their most promising shapes, as calculated by the Smith-Pierce method, were either very similar to bodies discussed herein, or were unsuitable for the present purpose.

Reference 13 was examined and its bibliography provided a good guide to some promising shapes.

The pressure distributions of those shapes that were calculated but not included in this report are available at the Model Basin.

The dimensionless offsets for the bodies discussed in this report are presented in Table I and the coordinate system is defined in Figure 1. Graphical comparisons of the forebodies and afterbodies are presented in Figures 2 and 3.

THE INCEPTION OF CAVITATION

If effects other than pressure* are neglected, cavitation on a body submerged in water will occur at any point on the surface of the body where the local pressure drops to the value of the vapor pressure of water. In the Bernoulli equation for frictionless flow, written for a free-stream point at the same depth as the submerged body and any point on the body,

$$p_A + p_H + 1/2\rho V^2 = p + 1/2\rho v^2$$

or $$\frac{p_A + p_H - p}{1/2\rho V^2} = \left(\frac{v}{V}\right)^2 - 1$$ where

p_A is the atmospheric pressure,

p_H is the free-stream pressure due to submergence,

p is the local pressure on the body,

ρ is the density of the water,

V is the free-stream velocity,

and v is the local velocity.

When the minimum pressure on the body drops to the vapor pressure of water ($p = p_V$) then

$$\frac{p_A + p_H - p_V}{1/2\rho V^2} = \sigma_i$$

defines the incipient-cavitation number. Hence, $\sigma_i = \left(\frac{v}{V}\right)^2_{max} - 1$. The problem of finding a body with high cavitation-inception speed reduces to finding a body with a minimum peak value of $\left(\frac{v}{V}\right)^2$.

The $\left(\frac{v}{V}\right)^2$ form chosen for presenting the potential velocity distribution data in this report conforms to the NACA method of presenting airfoil data.

Velocity distribution curves for the entire lengths of the bodies of revolution are presented. In addition, values of $\left(\frac{v}{V}\right)^2$ greater than 1.0

* For an account of other factors affecting the inception of cavitation see References 13 and 14.

are presented on a more precise scale since these values are of greater interest with regard to cavitation inception.

METHOD OF CALCULATING POTENTIAL VELOCITY DISTRIBUTIONS

The velocity distributions for the bodies of revolution discussed in this report were calculated by the method of Smith and Pierce.[3] They solved the Neumann boundary value problem for plane noncirculatory flows and flows with axial symmetry by using a surface source distribution and solving the resulting integral equation on a digital computer. A body of revolution moving in a direction parallel to its axis is a case of axially symmetric flow, and the Smith-Pierce method applies.

VERIFICATION OF METHOD OF CALCULATION

Analytical verification of the Smith-Pierce method is shown in Figure 4. The critical part of the analytical solution (from combining a three-dimensional doublet and rectilinear flow – see Reference 15) for a 27-inch diameter sphere is plotted using the same scale of $\left(\frac{v}{V}\right)^2$ as is used to present the velocity distribution data elsewhere in this report. The abscissa represents inches from the center of the 27-inch diameter sphere.

Three different cases were calculated for the sphere using the Smith-Pierce method:

1. Fifty-one equally spaced offsets correct to six significant figures. This corresponds to the precision of the offsets for the TMB-EPH form.

2. Fifty-one equally spaced offsets correct to five significant figures. This corresponds to the precision of the offsets for the Munzner-Reichardt bodies and the DTMB Series 58 bodies.

3. Fifty-one equally spaced offsets correct to four significant figures. This corresponds to the precision of the offsets for the NACA 16-series shapes.

It can be seen that the maximum theoretical error to be expected on smooth bodies whose shapes are defined by 51 equally spaced offsets correct

to 5 or 6 significant figures is about 0.3 percent, and on bodies correct to 4 significant figures, about 1.1 percent.

Experimental verification of the Smith-Pierce method may be seen in Figure 5. The measured values were obtained on DTMB Model 4198, a Series-58 model with L/D = 10, described in Reference 16. In the critical range of high velocity ratios, the discrepancy between the calculated and measured values of $\left(\frac{v}{V}\right)^2$ is approximately 0.1 percent. The discrepancy is less than 1 percent as far back as 80 percent of the length and increases to 3 percent in the region of 80-90 percent of length.

For bodies with blunt tails, viscosity causes appreciable separation at the tail and a concomitant divergence between potential theory values of pressure and measured values.

Goldstein[17] compares the experimental pressure distribution for a prolate spheroid with L/D = 4.0 with the distribution calculated from potential theory. Very good agreement exists between theory and experiment for approximately 95% of the length. The fact that this body has a blunter tail than any of the nacelle shapes discussed in this report indicates that the calculated pressures over the critical portions of the nacelle shapes can be assumed to be quite accurate.

However, for bodies with L/D less than 4.0, further comparisons would be required to determine the applicability of a potential theory calculation of pressure to that part of the shape that is critical.

DISCUSSION OF VELOCITY DISTRIBUTIONS AND DRAG

The potential velocity distributions for the five shapes with L/D = 5 are presented in Figure 6. More precise velocity distributions for the high velocity (low pressure) regions of each shape, with L/D = 5, 6, and 7, are presented in Figures 7, 8, and 9. This discussion concerns the bodies with L/D = 5.

The body having the lowest value of $\left(\frac{v}{V}\right)^2_{max}$ is the Munzner-Reichardt body. However, this shape has the disadvantage of a steep adverse pressure gradient near the tail. This will probably cause separation near the tail and a high drag. In Figure 10, incipient-cavitation number is plotted

against the corresponding free-stream velocity at which cavitation would first occur for a representative depth of submergence of 9 feet in salt water. (A curve for depth = 6 feet is included for reference.) In this figure, the effect of the finite water depth is considered only as it affects the ambient pressure. Distortion of the calculated flow streamlines due to the finiteness of the extent of the surrounding water is ignored. Cavitation may be expected to start on the Munzner-Reichardt body at 93.3 knots.

The DTMB Series 58 Model 4162 form (with altered L/D) has the next lowest value of $\left(\frac{v}{V}\right)^2$ and a dip in the $\left(\frac{v}{V}\right)^2$ curve in the midlength region where the maximum values of $\left(\frac{v}{V}\right)^2_{max}$ for a strut and foil would probably occur. Since the component maximum local velocities would occur at different lengthwise positions, they would be less likely to reinforce each other so strongly as they would if each component maximum velocity occurred at the same lengthwise position. The incipient-cavitation speed is 84.6 knots. Data from Reference 2 indicate that Model 4162 has acceptable drag at L/D = 7. Additional data are needed for lower fineness ratios.

The third lowest $\left(\frac{v}{V}\right)^2_{max}$ is that of the TMB-EPH. Its incipient-cavitation speed is 80.9 knots. Data from References 5 and 7 indicate that the drag of the TMB-EPH is comparable to the drag values of the bodies of Series 58 of the same fineness ratio.

The NACA 16-series body has a slightly higher $\left(\frac{v}{V}\right)^2_{max}$ than the TMB-EPH. Its incipient-cavitation speed is 78.1 knots. Though no drag data for a 16-series body of revolution are available, its pressure distribution indicates that this shape would be unlikely to have excessive separation. The systematic drag data in Reference 7 seem to confirm that this shape would have acceptable drag.

The DTMB Series 58 Model 4165 form (with altered L/D) has a cavitation-inception speed of 75.5 knots. In addition to the fairly high cavitation-inception speed, this form has very low drag.[2,7]

CONCLUSIONS

The most promising nacelle shape for use in combination with a hydrofoil and strut is the DTMB Series 58 Model 4162. It has the highest

theoretical cavitation-inception speed consistent with satisfactory drag characteristics. This nacelle appears suitable for use in combination with a strut and foil so placed that their maximum local velocities coincide with the midlength velocity dip on the nacelle.

The TMB-EPH is the most likely second choice, followed by the NACA 16-series and the DTMB Series 58 Model 4165. The Munzner-Reichardt shape would probably have excessive drag.

ACKNOWLEDGMENTS

The author wishes to thank Mr. Eugene P. Clement, Mr. Paul S. Granville, and Dr. Francis R. Hama of the David Taylor Model Basin for their advice and suggestions.

REFERENCES

1. Bureau of Ships letter SF 01 30 201 Serial 420-228 of 30 Aug 1960 to David Taylor Model Basin.

2. Clement, Eugene P. and Moore, Wilburn, L., "Resistance Data and Potential Velocity Distributions for a Systematic Series of Streamlined Bodies of Revolution (Series 58) for Application to the Design of Hydrofoil Boat Nacelles," David Taylor Model Basin Report C-1382 (Apr 1962) CONFIDENTIAL

3. Smith, A.M.O. and Pierce, J., "Exact Solution of the Neumann Problem. Calculation of Non-circulatory Plane and Axially Symmetric Flows About or Within Arbitrary Boundaries," Douglas Aircraft Co. Report No. E.S. 26988 (Apr 1958).

4. Munzner, H. and Reichardt, H., "Axially Symmetric Source - Sink Bodies with Predominantly Constant Pressure Distributions," U.S. Naval Ordnance Test Station Technical Memorandum 808-43 (Oct 1950).

5. Cauldwell, F.S. and Olson, C.R., "Resistance and Propulsion Characteristics of the High-Submerged-Speed Submarine, SST Schemes 1 and 2," David Taylor Model Basin Report C-343 (Sep 1950) CONFIDENTIAL.

6. Abbott, I.H. and von Doenhoff, A.E., "Theory of Wing Sections," McGraw-Hill Book Co., Inc., New York (1949).

7. Gertler, M., "Resistance Experiments on a Systematic Series of Streamlined Bodies of Revolution - For Application to the Design of High-Speed Submarines," David Taylor Model Basin Report C-297 (Apr 1950) CONFIDENTIAL.

8. Young, A.D. and Owen, P.R., "A Simplified Theory for Streamline Bodies of Revolution and its Application to the Development of High-Speed Low-Drag Shapes," ARC Technical Report R & M, No. 2071 (July 1943).

9. Young, A.D. and Young, E., "A Family of Streamline Bodies of Revolution Suitable for High-Speed or Low-Drag Requirements," ARC Technical Report R & M, No. 2204 (Aug 1945).

10. Neumark, S., "Velocity Distribution on Thin Bodies of Revolution at Zero Incidence in Incompressible Flow," ARC Technical Report R & M, No. 2814 (Jul 1950).

11. Brand, M., "Pressure Distributions over Bodies of Revolution for Axial Flow," David Taylor Model Basin Translation 220 (Apr 1947).

12. Loftin, L.K., Jr., "Theoretical and Experimental Data for a Number of NACA 6A-Series Airfoil Sections," NACA Report No. 903 (1948).

13. Breslin, J.P. and Landweber, L., "A Manual for Calculation of Inception of Cavitation on Hydrofoils and Bodies of Revolution," Stevens Institute of Technology Technical Memorandum No. 126 (May 1960).

14. Eisenberg, Phillip, "On the Mechanism and Prevention of Cavitation," David Taylor Model Basin Report 712 (Jul 1950).

15. Valentine, H.R., "Applied Hydrodynamics," Butterworths Scientific Publications, London (1959).

16. Beveridge, John L., "The Effect of Propeller Diameter on the Propulsive Efficiency Factors of a Single-Screw Submerged Body of Revolution," David Taylor Model Basin Report C-787 (Jan 1958) CONFIDENTIAL.

17. Goldstein, S. (ed.), "Modern Developments in Fluid Dynamics," Oxford University Press, London (1938), page 524, Vol. II.

TABLE 1

Dimensionless Offsets - Forebody

X/L	Y/Y_{max}				
	4165	16	4162	EPH	M-R
.00	.0000	.0000	.0000	.0000	.0000
.02	.2847	.2720	.2836	.2994	.3462
.04	.4041	.3655	.4010	.4184	.4581
.06	.4953	.4555	.4896	.5062	.5377
.08	.5710	.5210	.5623	.5772	.6008
.10	.6359	.5762	.6241	.6372	.6533
.12	.6925	.6250	.6775	.6889	.6983
.14	.7422	.6685	.7241	.7341	.7376
.16	.7860	.7080	.7649	.7740	.7721
.18	.8245	.7440	.8007	.8094	.8028
.20	.8583	.7773	.8322	.8408	.8303
.22	.8877	.8065	.8598	.8686	.8549
.24	.9131	.8335	.8840	.8932	.8769
.26	.9348	.8585	.9051	.9148	.8966
.28	.9531	.8825	.9235	.9337	.9142
.30	.9680	.9029	.9393	.9500	.9299
.32	.9799	.9220	.9530	.9639	.9438
.34	.9889	.9380	.9646	.9754	.9560
.36	.9952	.9525	.9743	.9846	.9665
.38	.9988	.9648	.9823	.9917	.9756
.40	1.0000	.9758	.9888	.9966	.9832
.42	.9988	.9845	.9937	.9993	.9893
.44	.9955	.9917	.9972	1.0000	.9940
.46	.9899	.9960	.9993	.9985	.9973
.48	.9823	.9980	1.0000	.9949	.9993
.50	.9728	1.0000	.9993	.9893	1.0000

TABLE 1 (Concluded)

Dimensionless Offsets - Afterbody

X/L	Y/Y_{max}				
	4165	16	4162	EPH	M-R
.50	.9728	1.0000	.9993	.9893	1.0000
.52	.9613	.9990	.9971	.9815	.9993
.54	.9480	.9970	.9934	.9716	.9973
.56	.9328	.9920	.9881	.9597	.9940
.58	.9159	.9832	.9811	.9456	.9893
.60	.8973	.9724	.9722	.9294	.9832
.62	.8769	.9600	.9613	.9111	.9756
.64	.8548	.9440	.9482	.8907	.9665
.66	.8309	.9250	.9328	.8683	.9560
.68	.8052	.9030	.9147	.8437	.9438
.70	.7778	.8782	.8939	.8170	.9299
.72	.7486	.8496	.8701	.7882	.9142
.74	.7174	.8177	.8429	.7573	.8966
.76	.6843	.7830	.8123	.7243	.8769
.78	.6491	.7435	.7779	.6892	.8549
.80	.6118	.6998	.7395	.6520	.8303
.82	.5723	.6520	.6968	.6126	.8028
.84	.5303	.6000	.6495	.5712	.7721
.86	.4858	.5445	.5972	.5277	.7376
.88	.4386	.4845	.5398	.4821	.6893
.90	.3882	.4196	.4768	.4341	.6533
.92	.3345	.3510	.4078	.3828	.6008
.94	.2765	.2760	.3322	.3267	.5377
.96	.2130	.1925	.2490	.2628	.4581
.98	.1398	.0995	.1554	.1830	.3462
1.00	.0000	.0000	.0000	.0000	.0000

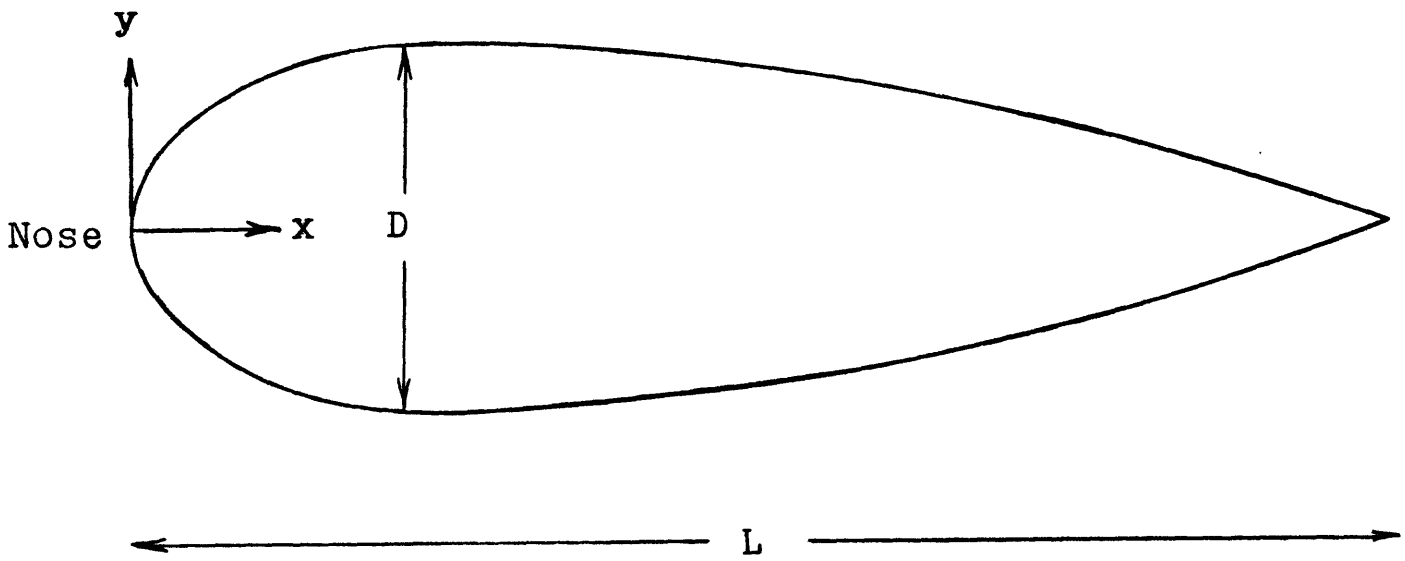

Figure 1 - Coordinate System for Bodies of Revolution

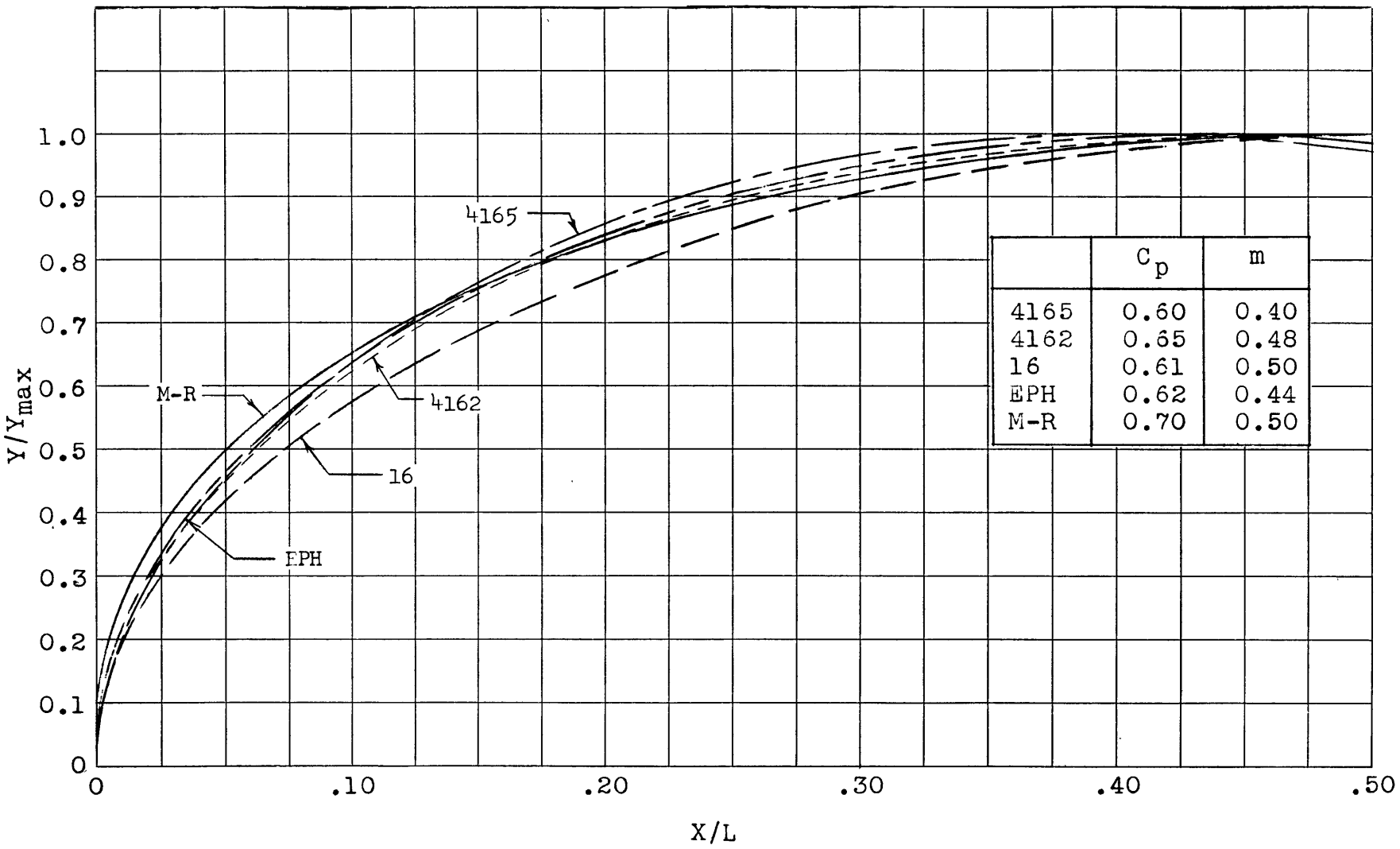

Figure 2 - Comparison of Forebody Shapes

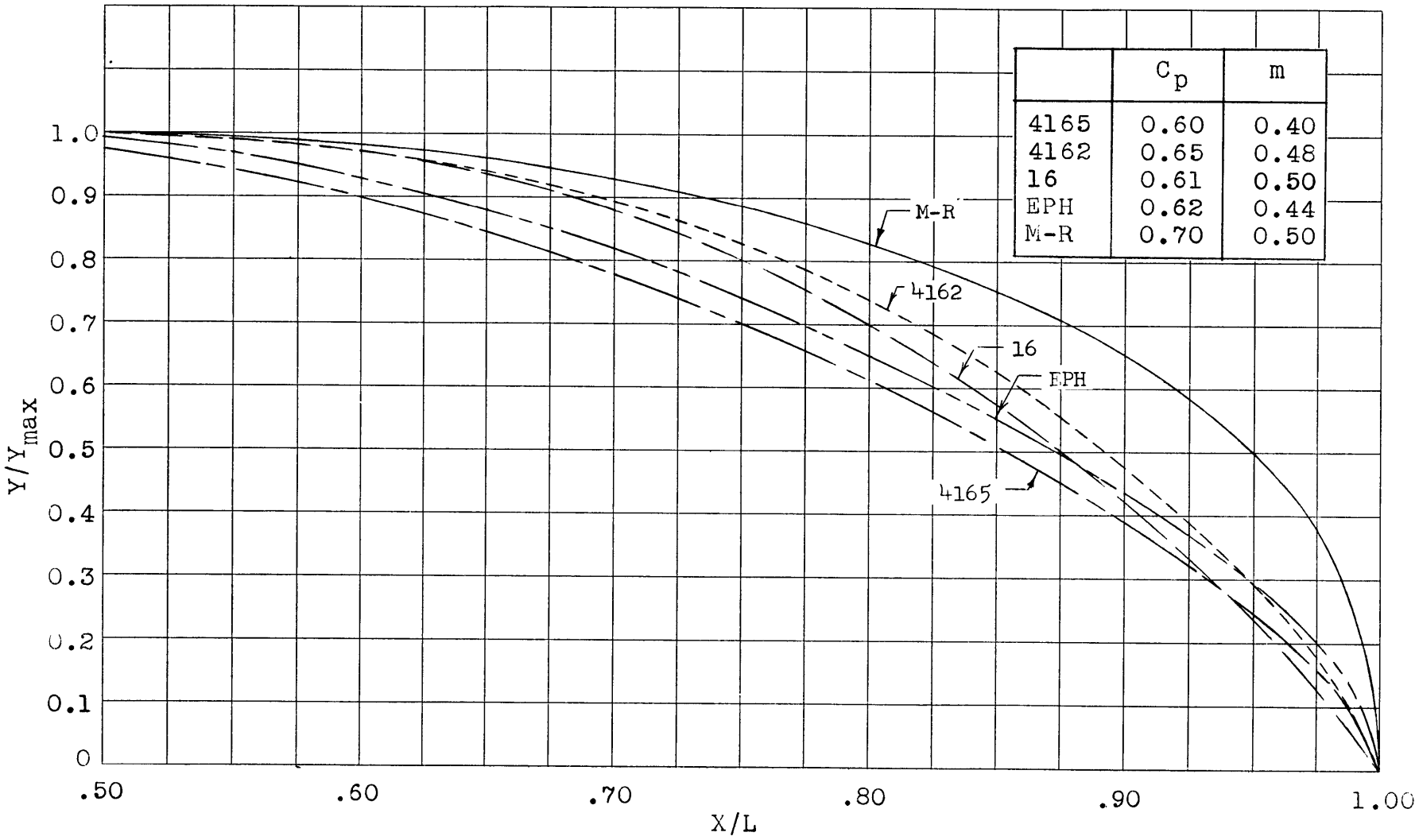

Figure 3 - Comparison of Afterbody Shapes

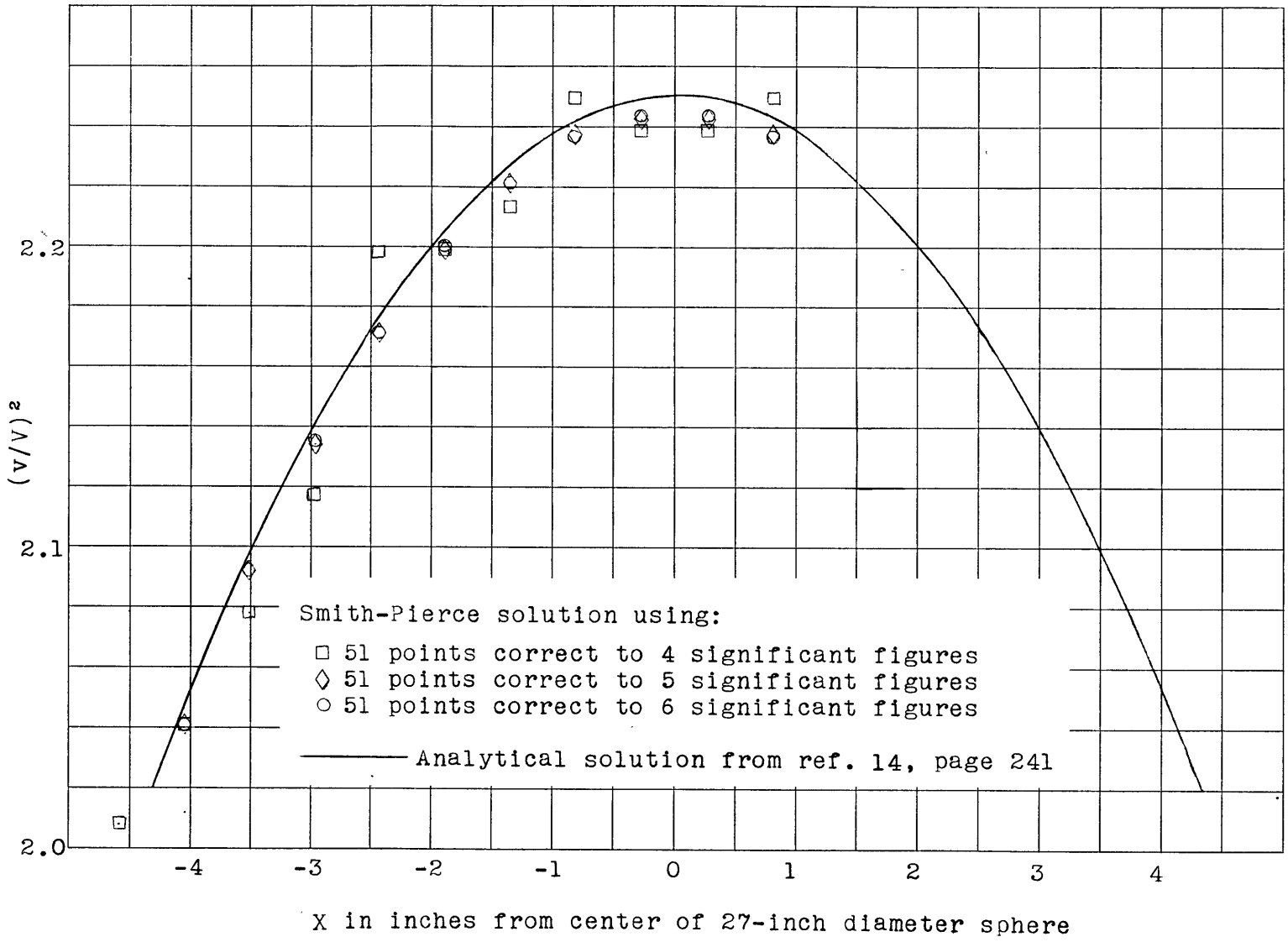

Figure 4 - Comparison of Smith-Pierce Method with Analytical Solution of Sphere

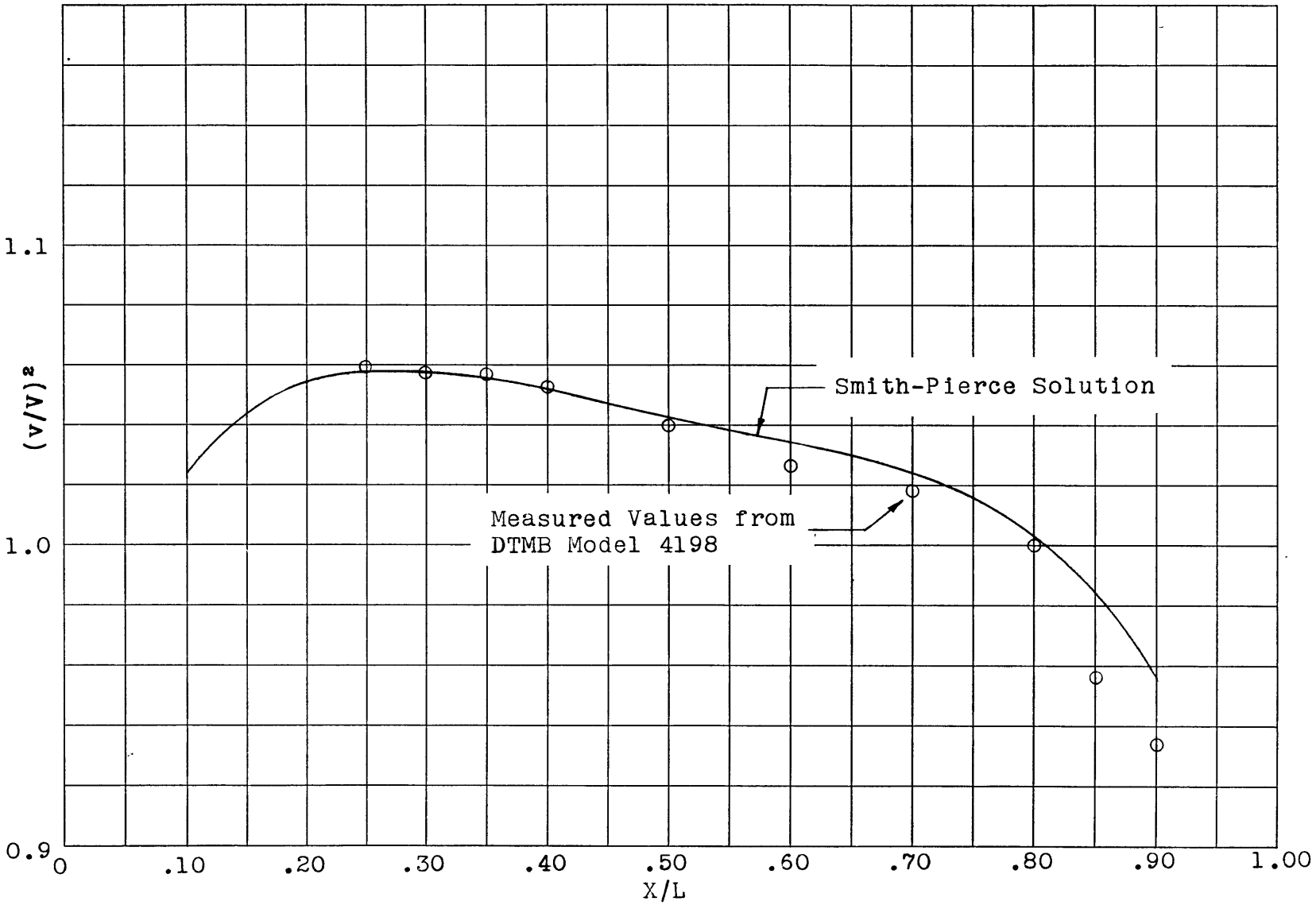

Figure 5 - Comparison of Smith-Pierce Method with Measured Results for a Streamlined Body of Revolution

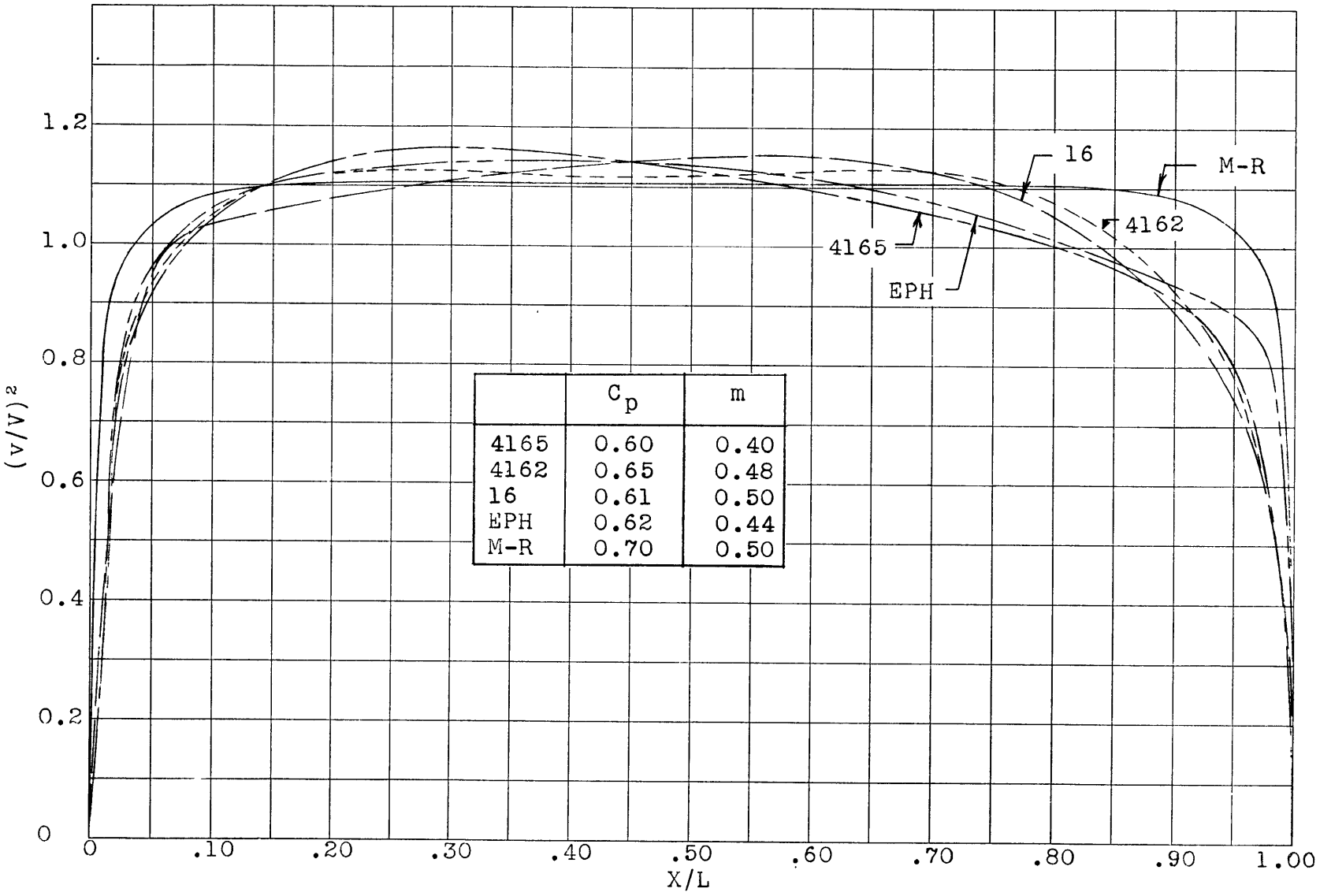

Figure 6 - Potential Velocity Distributions for Bodies with L/D=5.0

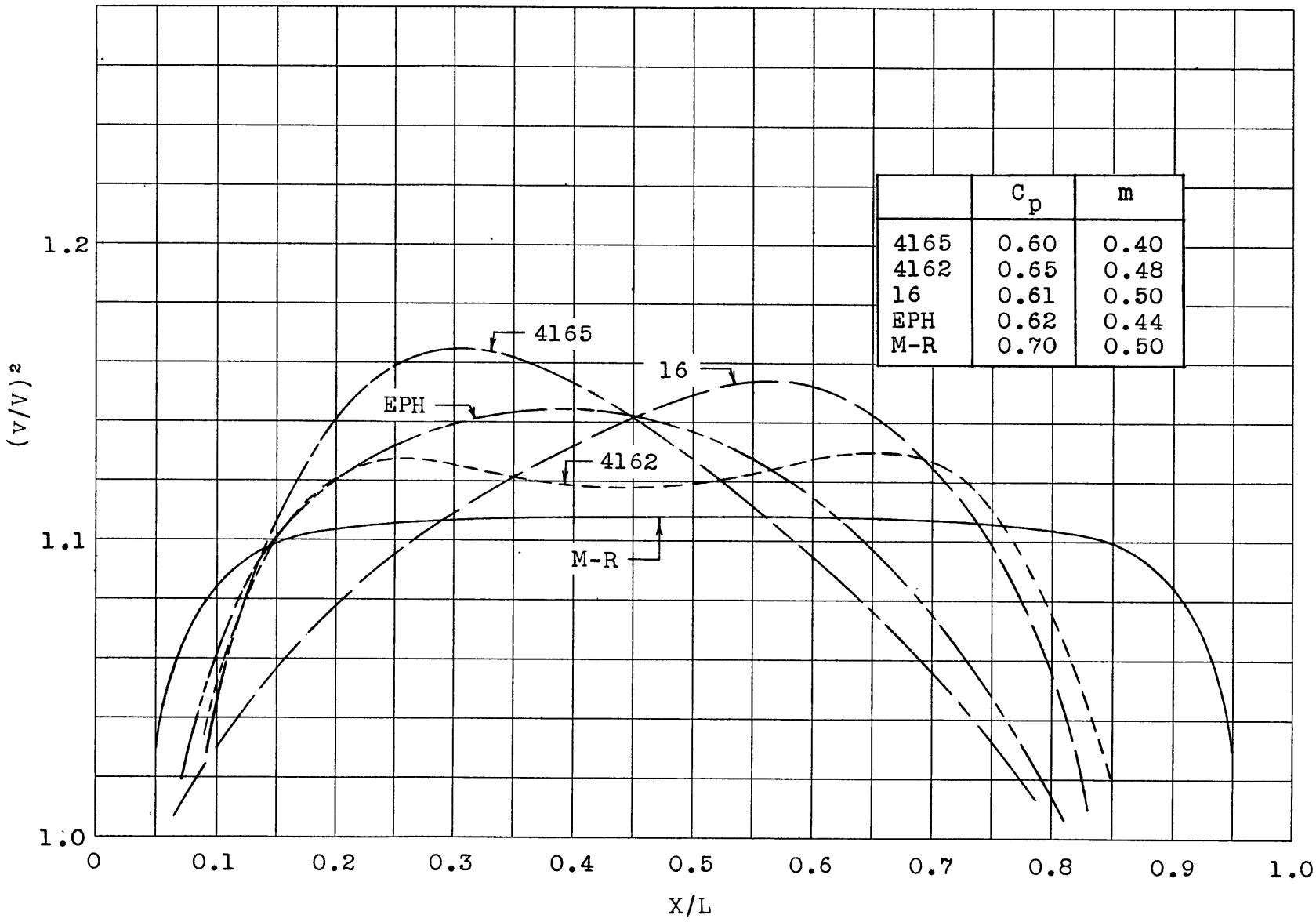

Figure 7 - Potential Velocity Distributions of Low Pressure Regions of Bodies with L/D=5.0

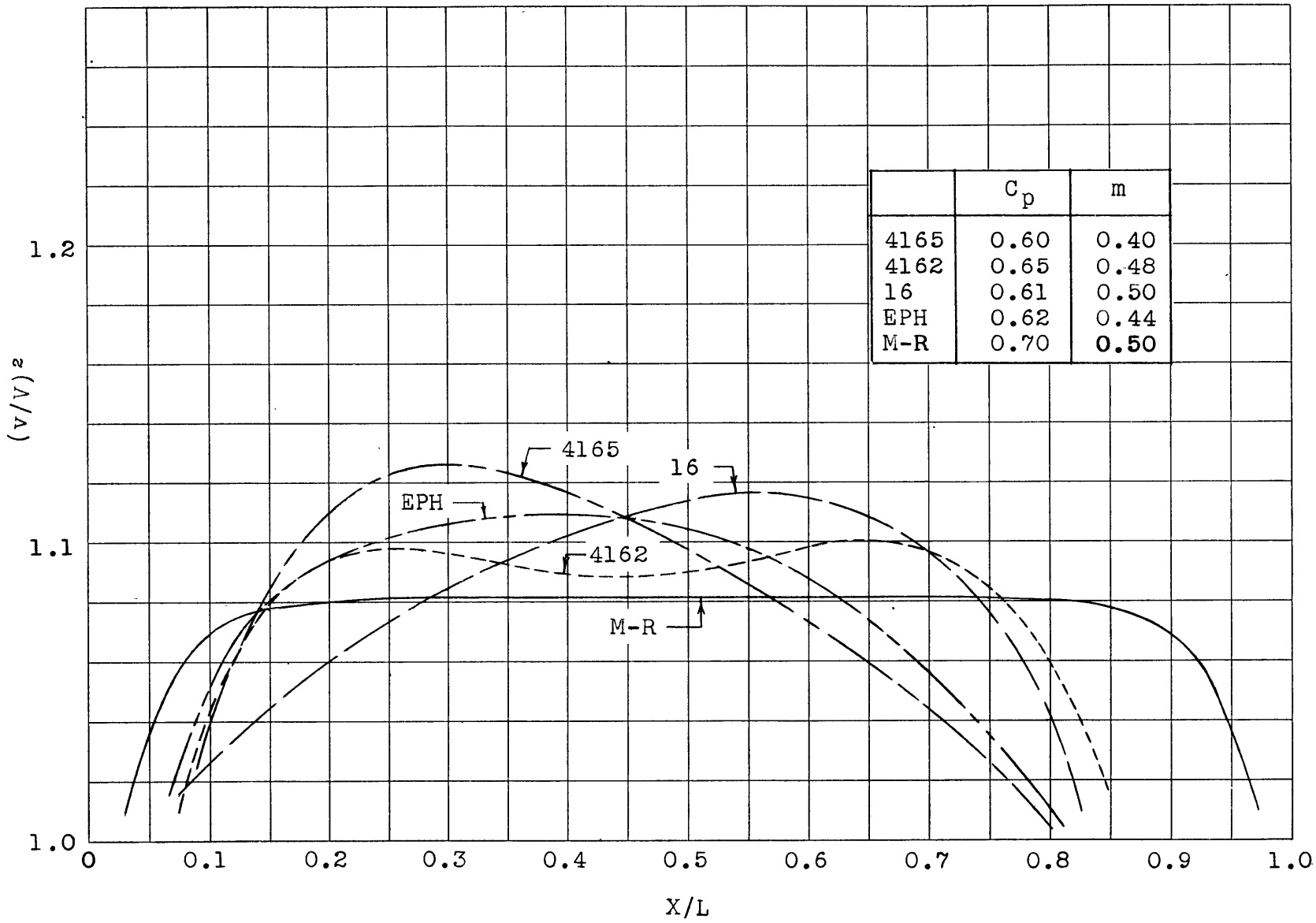

Figure 8 - Potential Velocity Distributions of Low Pressure Regions of Bodies with L/D=6.0

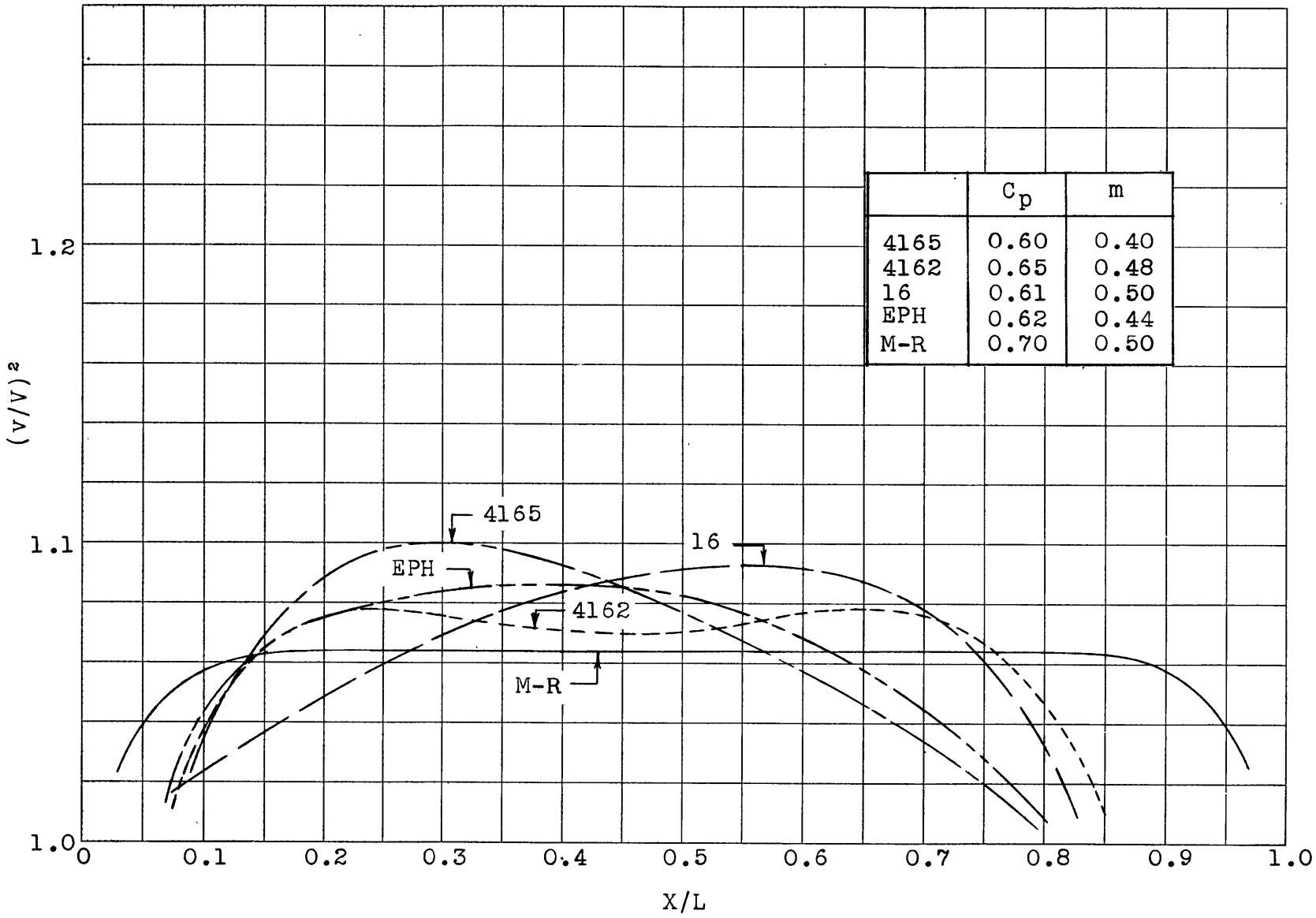

Figure 9 - Potential Velocity Distributions of Low Pressure Regions of Bodies with L/D=7.0

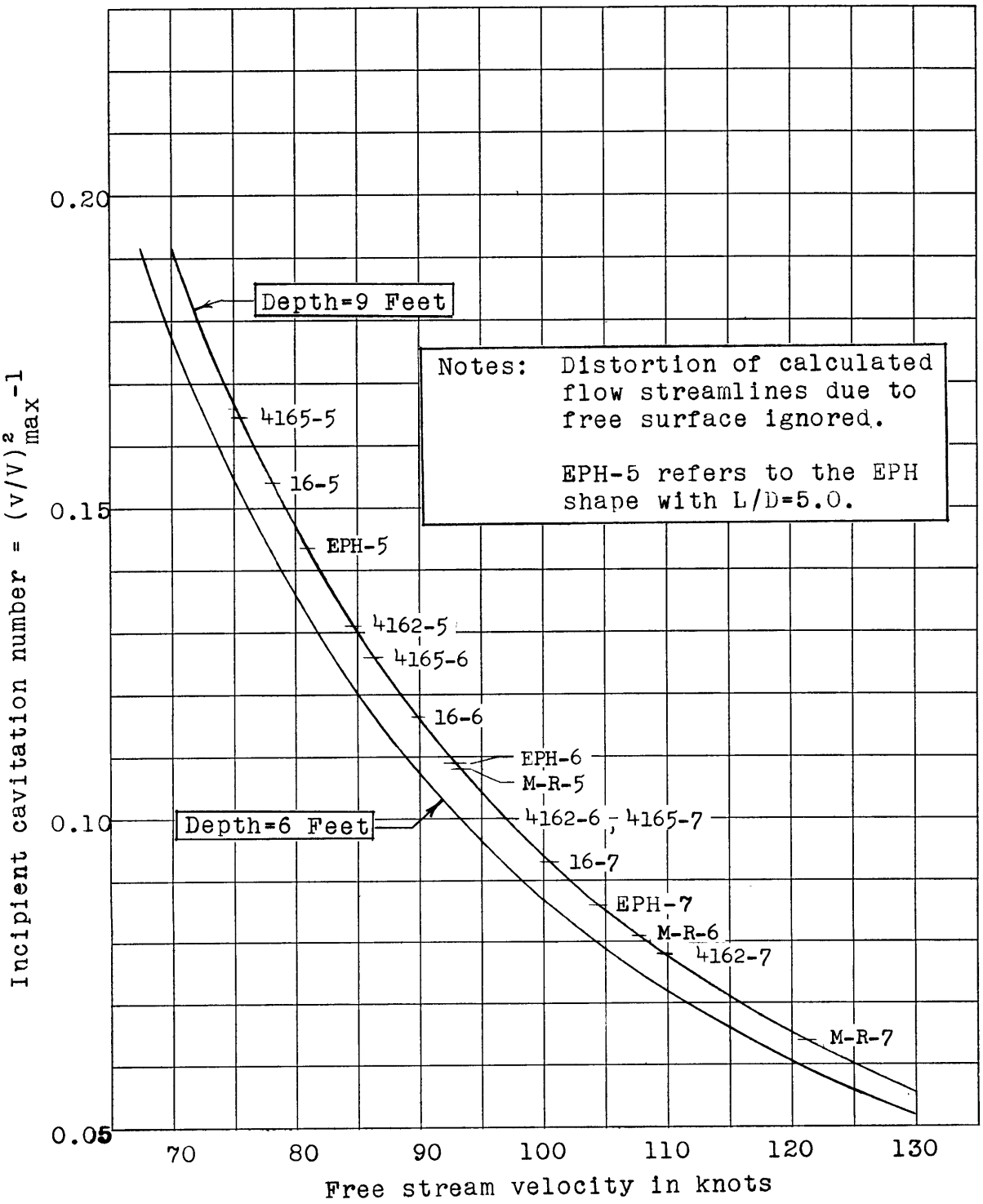

Figure 10 - Incipient Cavitation Number vs. Free-Stream Velocity at Inception of Cavitation in Salt Water at 59° F

INITIAL DISTRIBUTION

Copies	
9	CHBUSHIPS
	3 Tech Info Br (Code 335)
	1 Lab Mgt Div (Codd 320)
	1 Ship Silencing Br (Code 345)
	2 Prelim Des Br (Code 420)
	1 Sci & Res Sec (Code 442)
	1 Boats and Small Craft Sec (Code 449)
1	CHONR, Flu Dyn Br (Code 438)
1	CNO, Sur Prog Br (OP 712) Attn Capt. N.H. Fisher
1	DIR, Langley RESCENHYDRODIV, Attn Mr. John B. Parkinson
10	ASTIA
1	CDR, USNOTS, Pasadena Annex
1	Aero-Space Div, Boeing Airplane Co., Seattle
2	Hydro Lab, CIT, Pasadena
1	Hydro Res Lab, Convair Div, Genl Dyn Corp., San Diego
1	DIR, DL, SIT, Hoboken
1	Marine Engin Sec, Grumman Aircraft Engin Corp., Bethpage, Long Island
1	Hydronautics, Inc., Rockville
1	Head, Dept NAME, MIT, Cambridge
1	DIR, St Anthony Falls Hydraulic Lab, Univ of Minn, Minneapolis
1	SWRI, San Antonio, Attn H.N. Abramson, Dir, Mechanical Sci
1	TRG, Syosset, New York
1	DIR, Iowa Inst of Hydraulic Res, Univ of Iowa, Iowa City
1	Aerojet Genl Corp., Azusa, Attn Mr. J. Levy
1	Stanford Univ, Stanford, Attn Dr. B. Perry
1	Inst of Engin Res, Univ of Calif, Berkeley, Attn Prof. R. Paulling
1	Hydro Gp, Lockheed Aircraft Corp., Sunnyvale, Attn Mr. R.W. Kermeen